Performance of Self-Expanding Nitinol Stent in a Curved Artery: Impact of Stent Length and Deployment Orientation

Shijia Zhao
Department of Mechanical and Materials Engineering, University of Nebraska-Lincoln, Lincoln, NE, 68588-0656

Linxia Gu[1]
Department of Mechanical and Materials Engineering, University of Nebraska-Lincoln, Lincoln, NE 68588-0656; Nebraska Center for Materials and Nanoscience, Lincoln, NE, 68588-0656
e-mail: lgu2@unl.edu

Stacey R. Froemming
Hybrid Catheterization and Electrophysiology Laboratory, Children's Hospital and Medical Center, Omaha, NE, 68114-4133

The primary aim of this work was to investigate the performance of self-expanding Nitinol stents in a curved artery through finite element analysis. The interaction between a PROTÉGÉ™ GPS™ self-expanding Nitinol stent and a stenosed artery, as well as a sheath, was characterized in terms of acute lumen gain, stent underexpansion, incomplete stent apposition, and tissue prolapse. The clinical implications of these parameters were discussed. The impact of stent deployment orientation and the stent length on the arterial wall stress distribution were evaluated. It was found that the maximum principal stress increased by 17.46%, when the deployment orientation of stent was varied at a 5 deg angle. A longer stent led to an increased contact pressure between stent and underlying tissue, which might alleviate the stent migration. However, it also caused a severe hinge effect and arterial stress concentration correspondingly, which might aggravate neointimal hyperplasia. The fundamental understanding of the behavior of a self-expanding stent and its clinical implications will facilitate a better device design. [DOI: 10.1115/1.4007095]

Keywords: self-expanding stent, Nitinol, curved artery, stent-artery interaction, stent underexpansion, acute lumen gain, incomplete stent apposition, tissue prolapse

1 Introduction

Self-expanding Nitinol stents are increasingly popular in treating arterial occlusions, especially peripheral arterial disease. However, long-term patency of a stented vessel remains a challenge due to tissue ingrowth through the mesh structure of metal stents. The mechanism of arterial reocclusion is not yet fully understood. It is speculated that many factors, such as excessive stretch of the arterial wall, stent underexpansion, incomplete stent apposition (ISA), dimension and tortuosity of the artery contribute to the occurrence of reocclusion [1–3]. Evaluation of the mechanics of stent deployment and its interactions with diseased lesion will provide a fundamental understanding of stent dynamics and mechanical changes in the vessel wall.

Finite element method (FEM) has proven to be a very efficient and effective tool for the study of balloon-expandable stents, such as stent deployment and stent–artery interactions [4–9]. The interaction between self-expanding stents and arteries has undergone far less investigation using FEM. Moreover, most computational studies available in the literature focus on idealized straight vessels. Kleinstreuer et al. [10] simulated two Nitinol stent grafts to treat the abdominal aortic aneurysm in a straight vessel. Migliavacca et al. [11] compared stainless steel and Nitinol stents deployed into a straight coronary artery with a simplified cylindrical plaque. Several studies deployed a Nitinol stent into an anatomically accurate artery; however, plaque was not taken into account [12,13]. Wu et al. [14] simulated the delivery and release of Nitinol stent in a curved carotid artery; however, an idealized cylindrical plaque, corresponding to a 33% stenosis, was considered, which is usually not clinically significant for stent implantation. The effects of the stent deployment technique are also lacking in the documented finite element models. In addition, there is growing clinical evidence that self-expanding stents extend the duration of patency after treating the stenosed vessel, particularly when compared with balloon-mounted stents [15]. Therefore, better modeling of the deployment of the Nitinol stent and its interaction with curved stenosed artery will improve predictions of the stent performance and the design of a new generation of stents. The aim of this study is to systematically determine the behavior of a PROTÉGÉ™ GPS™ self-expanding stent (ev3 Inc., Plymouth, MN, USA) in a curved artery. The detailed interaction between stent, plaque and artery, the influence of stent deployment orientation and stent length on the level of the injury are presented and discussed.

2 Material and Methods

2.1 Geometry. A curved artery with 50% stenosis, based on the corresponding clinical study [16], was considered in this work (Fig. 1). The reference lumen dimensions are 9 mm in diameter, 1 mm in thickness, and 0.05 mm^{-1} in curvature [17]. The arc central angle between two ends of artery is 90 deg, which produces an arc length of 31.4 mm at the central line of artery. An asymmetric plaque which produces eccentric lumen [18] was attached onto the inner surface of artery, and the arc length at inner surface of

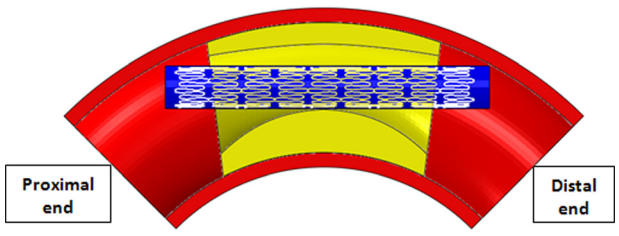

Fig. 1 Sectional view of the sheath-restrained Nitinol stent in a curved artery

[1]Corresponding author.

Contributed by the Bioengineering Division of ASME for publication in the JOURNAL OF BIOMECHANICAL ENGINEERING. Manuscript received January 12, 2012; final manuscript received June 3, 2012; accepted manuscript posted July 6, 2012; published online July 17, 2012. Assoc. Editor: Tim David.

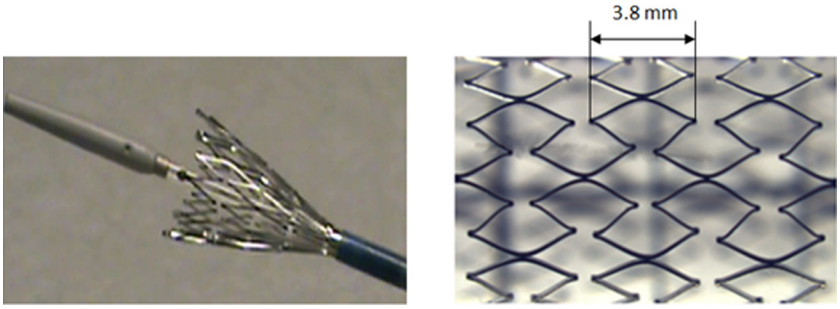

Fig. 2 PROTÉGÉ™ GPS™ self-expanding Nitinol stent partially deployed from the sheath and its microscopic image

plaque is around 16 mm. The PROTÉGÉ™ GPS™ self-expanding Nitinol stent was constrained by a sheath and delivered to the lesion site (Fig. 2). There are 16 units along the circumferential direction and nine units along the axial direction in the configuration of the stent, which led to a nominal diameter of 10 mm, length of 20 mm, and strut thickness of 0.22 mm.

2.2 Material Properties. The material properties of both the artery and plaque were described using a hyperelastic isotropic constitutive model. Uniaxial tension tests were performed on both axial and circumferential strips of human aorta obtained from a commercial 10 mm CryoValve® aortic root (CryoLife Inc., Kennesaw, GA, USA). A third order polynomial strain energy density function is used to fit the test data as,

$$U = \sum_{i+j=1}^{3} C_{ij}(I_1 - 3)^i (I_2 - 3)^j$$

where C_{ij} are material coefficients determined from the experimental data, while I_1 and I_2 are the first and second invariants of the Cauchy-Green tensor, defined as $I_1 = \lambda_1^2 + \lambda_2^2 + \lambda_3^2$ and $I_2 = \lambda_1^{-2} + \lambda_2^{-2} + \lambda_3^{-2}$, where λ_i are the principal stretches.

The coefficient of determination R^2 is used to measure how well the least squares equation predicts the experiential data. The higher the R^2, the more reliable the predictions obtained from the fitted model. The calculated R^2 is 0.925 for a reduced third order polynomial material model; while it is 0.753 for a reduced second order polynomial model fitting. Figure 3 clearly shows a better fit for the reduced third order polynomial model, which was used in this work. The obtained nonzero material coefficients are $C_{10} = 0.0104673$ MPa, $C_{20} = 0.0194098$ MPa, and $C_{30} = 0.0109830$ MPa. The material properties of plaque were adopted from the documented literatures [11], where a third order polynomial strain energy density function, with nonzero coefficients $C_{10} = 0.04$ MPa, $C_{02} = 0.003$ MPa, and $C_{03} = 0.02976$ MPa, was used.

The GPS™ stent is made of Nitinol material, which exhibits superelasticity and is associated with the stress induced phase transformation between the austenite and martensite phases. When loaded such that the stent is crimped into the sheath, the Nitinol material transforms from austenite to martensite. The transformation is initiated from stress state σ_L^S and completed by the stress value σ_L^E for the complete transformation. The reverse phase transformation will start as the loading is reduced to loading σ_U^S, such as when the sheath is removed. The original austenite phase will be totally recovered when the stress is further reduced to loading σ_U^E. The material parameters for the superelastic behavior of Nitinol [19], listed in the Table 1, were implemented in the ABAQUS 6.10 (Dassault Systèmes Simulia Corp., Providence, RI, USA) user material subroutine (VUMAT). Figure 4 has demonstrated the Nitinol material behavior obtained from the ABAQUS model.

2.3 Modeling. The self-expanding Nitinol stent was first crimped into the sheath, a rigid thin shell with a length of 22 mm.

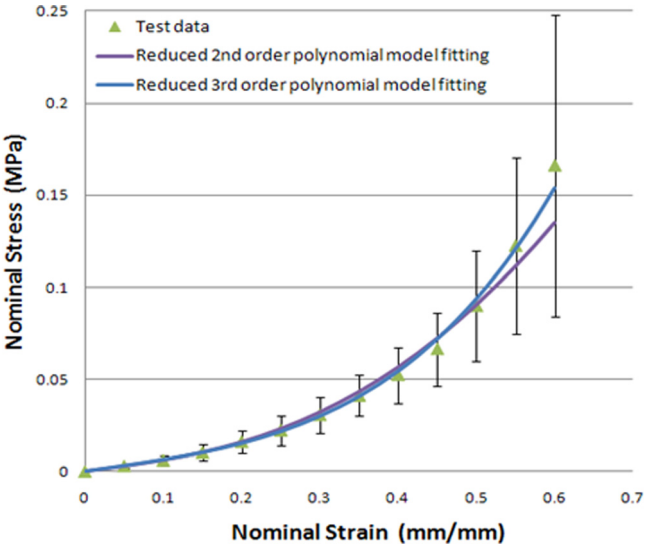

Fig. 3 The stress-strain relationship for artery

Table 1 Material parameters of Nitinol

Parameters	Description	Values
E_A	Austenite elasticity	46,728 MPa
ν_A	Austenite Poisson's ratio	0.33
E_M	Martensite elasticity	25,199 MPa
ν_M	Martensite Poisson's ratio	0.33
ε^L	Transformation strain	0.0426
σ_L^S	Start of transformation loading	358.2 MPa
σ_L^E	End of transformation loading	437.8 MPa
σ_U^S	Start of transformation unloading	124.25 MPa
σ_U^E	End of transformation unloading	17.75 MPa
σ_{CL}^S	Start of transformation stress (loading in compression)	537.3 MPa
ε_V^L	Volumetric transformation strain	0.0426

After the stent reached the targeted lesion site, a ramping velocity of 4000 mm/s was applied to remove the sheath along the axial direction. Thus the Nitinol stent was released and subsequently expanded to open the stenosed lumen. A finite-sliding, general contact formulation was adopted for the stent-tissue interactions. A friction coefficient of 0.05 was prescribed among all contact surfaces [20]. Artery and plaque were meshed with 17,784 and 8816 reduced eight-node brick elements (C3D8R), respectively. The GPS™ stent was discretized into 7248 two-node linear beam elements (B31), which accounts for large axial strains as well as transverse shear strains. The sheath is discretized with 988 reduced four-node shell elements (S4R).

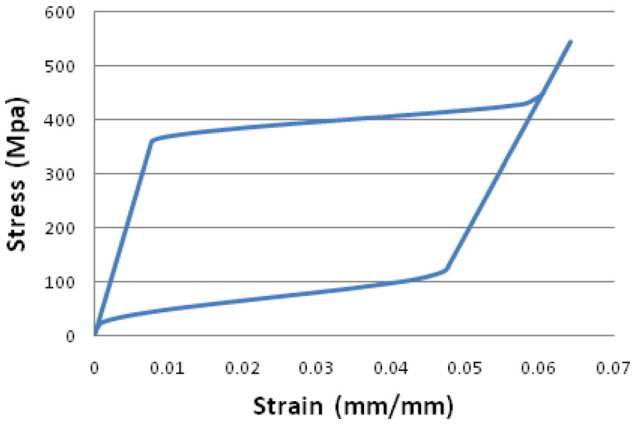

Fig. 4 The hysteresis behavior of Nitinol obtained from ABAQUS

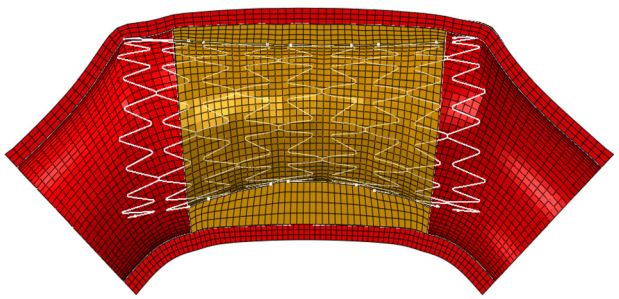

Fig. 5 The deformation of the artery, plaque, and stent in the curved stenosed artery

3 Results

The GPS^{TM} Nitinol stent restored patency in a curved vessel with 50% stenosis, as shown in Fig. 5. After stenting, the stent length is 21.77 mm, compared with the original length of 20 mm. The diameter of the stent is 7.72 mm at the center of the plaque, 10.01 mm at the proximal end of the stent, and 10.04 mm at the distal end of the stent, respectively. This indicates a possible stent underexpansion, evaluated as the ratio of minimum stent area to the mean proximal and distal reference lumen area [21]. Underexpansion occurs if this ratio is less than 80% [21]. In this work, the minimum lumen cross-sectional area enclosed by the stent is calculated as 50.22 mm^2 while the proximal and distal reference lumen area are 91.78mm^2 and 87.38 mm^2, respectively. The corresponding ratio is 56.06%, which indicates the presence of underexpansion. Underexpansion usually leads to noncontact regions between the stent and artery wall, also referred to as incomplete stent apposition (ISA) [22]. The stent strut is not fully flush against the wall, and hence a lack of contact between the strut and the underlying arterial wall. An ISA area of 160.55 mm^2 is obtained in our model.

Acute lumen gain, quantified as the increase in lumen diameter, is a positive indicator of stent performance. The minimum lumen diameter increased from the initial 4.5 mm to 7.61 mm, which corresponded to a 15.44% residual stenosis after stenting, as illustrated in Fig. 6 and Table 2. The variable D refers to the inner diameter of the artery, and t_{max}, t_{min} refer to the limit thickness of the plaque at one cross-section. An acute lumen gain is calculated as 3.11 mm due to plaque compressions and arterial wall stretching. It is clear that the stented artery is stretched by 23.44%, and reaches to an inner diameter of 11.11 mm at the site of narrowest occlusion. The plaque, however, was compressed by 0.63 mm (Δt_{max}) and 0.37 mm (Δt_{min}), respectively, which indicates a 21.00% compression in the thick side of the plaque, and 24.67% compression in the thin side of the plaque. Similar compressions are also observed at both plaque ends with around 22% arterial stretch. In our case, arterial wall stretch contributes to approximately 68% of the lumen gain at the site of narrowest occlusion; in addition to plaque compression and redistribution.

Acute lumen gains are compromised by tissue prolapse, estimated as the maximal protrusion of the arterial tissue between stent struts. The tissue prolapse, defined as the relative radial distance between the protruded tissue and its surrounding strut, is 0.44 mm at maximum in the central cross-sections, which is larger than the stent strut thickness of 0.22 mm, indicating the lumen loss due to the draping of the tissue within the units of the stent. This may affect the hemodynamics and induce late stent thrombosis and in-stent restenosis [23].

Deployment of stent induced stress concentrations on the arterial wall, which contribute to the occurrence of in-stent restenosis. Figure 7(*a*) demonstrates that stent implantation straightened the curved vessel wall and that the stent ends poked into the artery, this phenomenon is referred to as the hinge effect. The effect of catheter tilting is estimated by inclining the crimped stent 5 deg

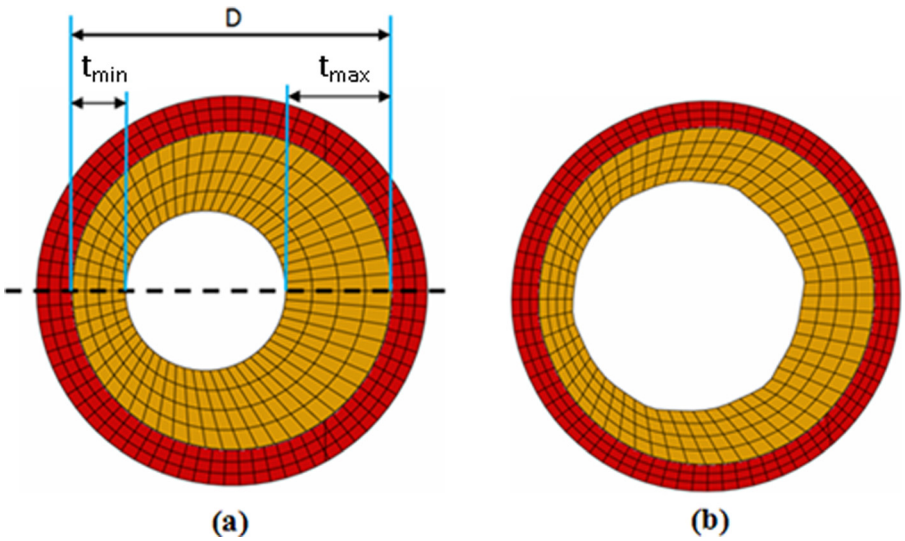

Fig. 6 The cross section of stenosed artery at site of narrowest occlusion. (*a*) before stenting; (*b*) after stenting. Where D denotes the inner diameter of the artery, t_{min} and t_{max} are the plaque thickness at its thin and thick side, respectively.

Table 2 Stent-induced variations in the geometry of stenosed artery

		t_{max} (mm)	t_{min} (mm)	D (mm)
Plaque center (narrowest occlusion)	Before stenting	3.00	1.50	9.00
	After stenting	2.37	1.13	11.11
Plaque ends	Before stenting	1.57	0.94	9.32
	After stenting (Proximal)	1.40	0.63	11.40
	After stenting (Distal)	1.45	0.66	11.33

counterclockwise against the initial center positioning (Fig. 7(*b*)). The maximum principal stress in the arterial wall increased from 0.063 MPa to 0.074 MPa after stent tilting. Meanwhile, the stent-induced distal hinge effect becomes more prominent. The maximum principal nominal strain at the distal end was elevated from 33.99% to 38.69%, which was a 13.83% increase due to the 5 deg orientation variation. It is natural to observe that the hinge effect was alleviated at the proximal end of the stent, where the maximum principal nominal strain at the hinge points decreased from 36.22% to 31.28%.

The influence of stent length is investigated by adding two or four more units onto the original stent, which has nine units alone axial direction. The stent with nine units along the axial direction was referred to as "Stent U9" and the ones with 11 or 13 units as "Stent U11" or "Stent U13," respectively. The lumen gain after stenting of "Stent U11" and "Stent U13" were 3.40 mm and 3.44 mm, respectively, comparing with 3.11 mm for the original "Stent U9." The maximum contact pressure between stent and underlying tissue for "Stent U9," "Stent U11," and "Stent U13" were 0.27 MPa, 0.31 MPa, and 0.45 MPa, respectively. The increased stent length also led to severe arterial stress concentrations, as shown in Fig. 8. The arterial volume where principal stress exceeds 0.06 MPa, the average blood pressure induced arterial stress level, were 0.01%, 2.54%, and 11.95% after deployment of "Stent U9," "Stent U11," and "Stent U13," respectively.

4 Discussion

In this study, the deployment of a self-expanding Nitinol stent in a curved artery is simulated to get a better fundamental understanding of the interaction between the stent and the stenosed artery, as well as its clinical implications. Both artery and plaque underwent considerable geometry change immediately after the deployment of Nitinol stent. This agrees with the documented clinical observations, which showed that arterial wall stretching and plaque compression are the two main contributors to lumen gain after stenting [24]. It is also clear that the thin side of plaque was compressed more than the thick side, which caused higher arterial stress contacting the thin side of plaque (Fig. 6 and Table 2). This may be explained by the lower resistance at the thin side of the plaque. A stenting study in rabbits showed a positive correlation between the extent of plaque or medial compression and the observed neointimal hyperplasia [25]. This implied that the varied medial compressions might lead to nonuniform thickening of the intima of the stented artery. Results show that Nitinol stents exhibit underexpansion immediately after its deployment. This is partially attributed to the lower stiffness of Nitinol as a material (47 GPa), compared with the conventional stainless steel material with a stiffness of 190 GPa. It is speculated that the underexpansion of bare metal stents is associated with thrombosis and the occurrence of restenosis [21,26–28]. Post balloon angioplasty after stent deployment is suggested by some researchers to reduce the underexpansion [29]. Other groups, however, have suggested that Nitinol stents will continue expanding to listed nominal diameter up to nine months after the deployment; thus acute underexpansion may be corrected by the stent itself due to its shape memory properties [30–32]. Late expansion of Nitinol stents may compensate the lumen loss caused by neointimal hyperplasia; however, it is at the expense of arterial overstretching [31,32].

This work has shown that underexpansion may lead to increased hinge effect at both ends of the stent, especially when the catheter is slightly tilted. The influence of tilted catheter can be extended to various arterial curvatures, but it is pronounced in arteries with larger curvatures. Considering the reality of catheter

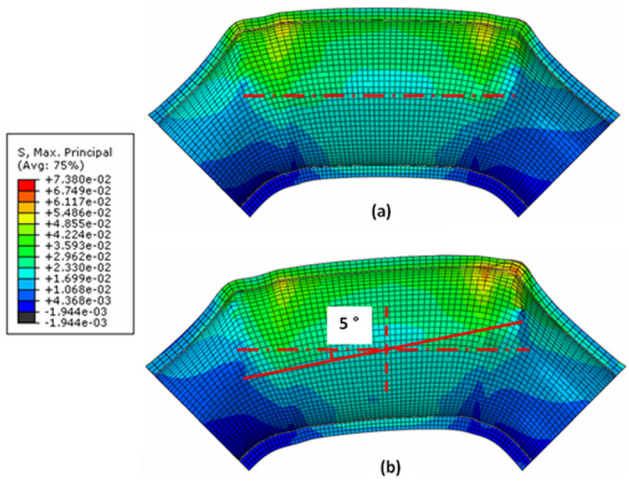

Fig. 7 Arterial stress distributions after stent deployment. (*a*) catheter along the center of the lumen; (*b*) tilted catheter with 5 deg angle counterclockwise.

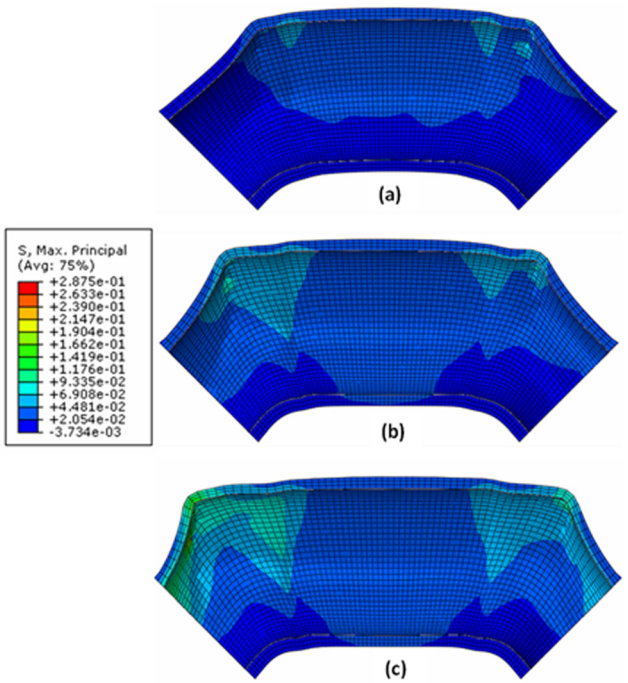

Fig. 8 The influence of stent length on arterial wall stress. (*a*) "Stent U9," (*b*) "Stent U11," and (*c*) "Stent U13".

position in a curved artery, the initial stent deployment orientation is rotated for 5 deg angle. The maximum principal nominal strain at the distal end increased by 13.83%, which indicates a more severe hinge effect. The hinge effect, due to the nonuniform asymmetric plaque, stent oversizing, and underexpansion, will cause higher local stresses and stress gradients on the artery. This may trigger neointimal proliferation at those locations, and contribute to the occurrence of restenosis [33]. Meanwhile, the peak stress gradient may lead to edge dissection, which requires further intervention [34,35]. Considering the smaller contact load at the stent ends, soft strut links at the ends of stents are suggested to alleviate these hinge effects [36].

The tortuosity of the stenosed artery was modified by the implanted stent. This is clearly demonstrated by the stented curved vessel. The nonuniform plaque profile caused noncontact regions between the stent and arterial wall. This implies that drug-eluting stents may sacrifice the drug effect on the artery, and blood stagnation may form in theseareas which may initiate thrombosis. It is speculated that more units with shorter struts will reduce the ISA area and increase the compliance of the stents used in tortuous artery [14].

The effect of stent length was evaluated in terms of contact pressure between stent and underlying tissue and the potential injury to the arterial wall. It is clear that a longer self-expanding stent enhances the contact pressure between stent and underlying tissue, which may reduce the stent migration [37]. The instant lumen gain was also improved with a longer stent that protrudes wide into the normal portions of the artery. However, the longer stent induced more severe hinge effect and much larger stress concentrations at the ends of the stents, which may increase the possibility of neointimal hyperplasia.

In this study, the baseline stenosis of 50% was adopted from the clinical studies of PROTÉGÉ^{TM} GPS^{TM} carotid stent [16]. For the stenting treatment of severe stenosis, i.e., 70% or greater, a balloon predilation was generally needed [30], which was not considered in this work. The material properties of artery and plaque are defined as homogeneous, isotropic, and hyperelastic, though they have been shown to be nonhomegeneous, anisotropic, and viscoelastic [38,39]. Hyperelastic constitutive equations were extensively used to describe the nonlinear stress-strain relationship for the elastic state of arterial tissue; however, the inelastic phenomena such as plastic or fracture-related deformation could not be addressed by the hyperelastic material model itself. Effects of blood flow and more realistic material models were not considered in this work. The superelasticity of Nitinol stents is considered to accommodate large strains in this work; however, its shape memory properties related to temperature driven deformation was neglected, which will become essential to model the late expansion. The geometry of the artery and plaque were idealized for this comparative study. An MRI reconstructed model may change the stress concentration on the arterial wall. With the advancement of finite element models, clinical treatment planning through finite element method could help to predict the clinical outcomes. In spite of these limitations, this study demonstrated the performance of Nitinol stents in a curved artery in terms of underexpansion, ISA, hinge effect, and stress concentration. The results obtained herein provide guidance for optimizing stent designs and potential clinical performance.

Acknowledgment

The authors are grateful for funding from the National Science Foundation under Grant Nos. 0926880 and 0811250.

References

[1] Gu, L. X., Zhao, S. J., Muttyam, A. K., and Hammel, J. M., 2010, "The Relation Between the Arterial Stress and Restenosis Rate After Coronary Stenting," J. Med. Devices, **4**(3), p. 031005.

[2] Kim, W., Jeong, M. H., Lee, S. R., Lim, S. Y., Hong, Y. J., Ahn, Y. K., and Kang, J. C., 2007, "An Accordion Phenomenon Developed After Stenting in a Patient With Acute Myocardial Infarction," Int. J. Cardiol., **114**(2), pp. E60–E62.

[3] Zhou, R. H., Lee, T. S., Tsou, T. C., Rannou, F., Li, Y. S., Chien, S., and Shy, J. Y., 2003, "Stent Implantation Activates AKT in the Vessel Wall: Role of Mechanical Stretch in Vascular Smooth Muscle Cells," Arterioscler., Thromb., Vasc. Biol., **23**(11), pp. 2015–2020.

[4] Bedoya, J., Meyer, C. A., Timmins, L. H., Moreno, M. R., and Moore, J. E., 2006, "Effects of Stent Design Parameters on Normal Artery Wall Mechanics," J. Biomech. Eng., **128**(5), pp. 757–765.

[5] Holzapfel, G. A., Stadler, M., and Gasser, T. C., 2005, "Changes in the Mechanical Environment of Stenotic Arteries During Interaction With Stents: Computational Assessment of Parametric Stent Designs," J. Biomech. Eng., **127**(1), pp. 166–180.

[6] Lally, C., Dolan, F., and Prendergast, P. J., 2005, "Cardiovascular Stent Design and Vessel Stresses: A Finite Element Analysis," J. Biomech., **38**(8), pp. 1574–1581.

[7] Zahedmanesh, H., Kelly, D. J., and Lally, C., 2010, "Simulation of a Balloon Expandable Stent in a Realistic Coronary Artery-Determination of the Optimum Modelling Strategy," J. Biomech., **43**(11), pp. 2126–2132.

[8] Pericevic, I., Lally, C., Toner, D., and Kelly, D. J., 2009, "The Influence of Plaque Composition on Underlying Arterial Wall Stress During Stent Expansion: The Case for Lesion-Specific Stents," Med. Eng. Phys., **31**(4), pp. 428–433.

[9] De Beule, M., Mortier, P., Carlier, S. G., Verhegghe, B., Van Impe, R., and Verdonck, P., 2008, "Realistic Finite Element-Based Stent Design: The Impact of Balloon Folding," J. Biomech., **41**(2), pp. 383–389.

[10] Kleinstreuer, C., Li, Z., Basciano, C. A., Seelecke, S., and Farber, M. A., 2008, "Computational Mechanics of Nitinol Stent Grafts," J. Biomech., **41**(11), pp. 2370–2378.

[11] Migliavacca, F., Petrini, L., Massarotti, P., Schievano, S., Auricchio, F., and Dubini, G., 2004, "Stainless and Shape Memory Alloy Coronary Stents: A Computational Study on the Interaction With the Vascular Wall," Biomech. Model. Mechanobiol., **2**(4), pp. 205–217.

[12] Conti, M., Auricchio, F., De Beule, M., and Verhegghe, B., 2009, "Numerical Simulation of Nitinol Peripheral Stents: From Laser-Cutting to Deployment in a Patient Specific Anatomy," Proceedings of the 8th European Symposium on Martensitic Transformations, Prague, Czech Republic.

[13] Rebelo, N., Fu, R., and Lawrenchuk, M., 2009, "Study of a Nitinol Stent Deployed into Anatomically Accurate Artery Geometry and Subjected to Realistic Service Loading," J. Mater. Eng. Perform., **18**(5–6), pp. 655–663.

[14] Wu, W., Qi, M., Liu, X. P., Yang, D. Z., and Wang, W. Q., 2007, "Delivery and Release of Nitinol Stent in Carotid Artery and their Interactions: A Finite Element Analysis," J. Biomech., **40**(13), pp. 3034–3040.

[15] Levy, E. I., Sauvageau, E., Hanel, R. A., Parikh, R., and Hopkins, L. N., 2006, "Self-Expanding Versus Balloon-Mounted Stents for Vessel Recanalization following Embolic Occlusion in the Canine Model: Technical Feasibility Study," Am. J. Neuroradiol., **27**(10), pp. 2069–2072.

[16] FDA(P060001), 2007, "Summary of Safety and Effectiveness Data (SSED), Protege® GPS^{TM} Carotid Stent System," ev3 Inc.

[17] Prosi, M., Perktold, K., Ding, Z., and Friedman, M. H., 2004, "Influence of Curvature Dynamics on Pulsatile Coronary Artery Flow in a Realistic Bifurcation Model," J. Biomech., **37**(11), pp. 1767–1775.

[18] De Franco, A. C., and Nissen, S. E., 2001, "Coronary Intravascular Ultrasound: Implications for Understanding the Development and Potential Regression of Atherosclerosis," Am. J. Cardiol., **88**(10A), pp. 7M–20M.

[19] Rebelo, N., Walker, N., and Foadian, H., 2001, "Simulation of Implantable Nitinol Stents," Proceedings of the 2001 Abaqus Users Conference, Providence, Rhode Island, USA.

[20] Dunn, A. C., Zaveri, T. D., Keselowsky, B. G., and Sawyer, W. G., 2007, "Macroscopic Friction Coefficient Measurements on Living Endothelial Cells," Tribol. Lett., **27**(2), pp. 233–238.

[21] Uren, N. G., Schwarzacher, S. P., Metz, J. A., Lee, D. P., Honda, Y., Yeung, A. C., Fitzgerald, P. J., and Yock, P. G., 2002, "Predictors and Outcomes of Stent Thrombosis: An Intravascular Ultrasound Registry," Eur. Heart J., **23**(2), pp. 124–132.

[22] Cheneau, E., Satler, L. F., Escolar, E., Suddath, W. O., Kent, K. M., Weissman, N. J., Waksman, R., and Pichard, A. D., 2005, "Underexpansion of Sirolimus-Eluting Stents: Incidence and Relationship to Delivery Pressure," Cathet Cardiovasc. Intervent., **65**(2), pp. 222–226.

[23] Farb, A., Burke, A. P., Kolodgie, F. D., and Virmani, R., 2003, "Pathological Mechanisms of Fatal Late Coronary Stent Thrombosis in Humans," Circulation, **108**(14), pp. 1701–1706.

[24] Albrecht, D., Kaspers, S., Fussl, R., Hopp, H. W., and Sechtem, U., 1996, "Coronary Plaque Morphology Affects Stent Deployment: Assessment by Intracoronary Ultrasound," Cathet. Cardiovasc. Diagn., **38**(3), pp. 229–235.

[25] Carter, A. J., Farb, A., Gould, K. E., Taylor, A. J., and Virmani, R., 1999, "The Degree of Neointimal Formation After Stent Placement in Atherosclerotic Rabbit Iliac Arteries is Dependent on the Underlying Plaque," Cardiovasc. Pathol., **8**(2), pp. 73–80.

[26] Cheneau, E., Leborgne, L., Mintz, G. S., Kotani, J., Pichard, A. D., Satler, L. F., Canos, D., Castagna, M., Weissman, N. J., and Waksman, R., 2003, "Predictors of Subacute Stent Thrombosis: Results of a Systematic Intravascular Ultrasound Study," Circulation, **108**(1), pp. 43–47.

[27] Duda, S. H., Wiskirchen, J., Tepe, G., Bitzer, M., Kaulich, T. W., Stoeckel, D., and Claussen, C. D., 2000, "Physical Properties of endovascular Stents: An Experimental Comparison," J. Vasc. Intervent. Radiol., **11**(5), pp. 645–654.

[28] Fujii, K., Carlier, S. G., Mintz, G. S., Yang, Y. M., Moussa, I., Weisz, G., Dangas, G., Mehran, R., Lansky, A. J., Kreps, E. M., Collins, M., Stone, G. W., Moses, J. W., and Leon, M. B., 2005, "Stent Underexpansion and Residual Reference Segment Stenosis are Related to Stent Thrombosis After Sirolimus-Eluting Stent Implantation: An Intravascular Ultrasound Study," J. Am. Coll. Cardiol., **45**(7), pp. 995–998.
[29] Romagnoli, E., Sangiorgi, G. M., Cosgrave, J., Guillet, E., and Colombo, A., 2008, "Drug-Eluting Stenting: The Case for Post-Dilation," J. Am. Coll. Caridol.: Cardiovasc. Intervent., **1**(1), pp. 22–31.
[30] Lownie, S. P., Pelz, D. M., Lee, D. H., Men, S., Gulka, I., and Kalapos, P., 2005, "Efficacy of Treatment of Severe Carotid Bifurcation Stenosis by Using Self-Expanding Stents Without Deliberate Use of Angioplasty Balloons," Am. J. Neuroradiol., **26**(5), pp. 1241–1248.
[31] Sanmartin, M., Goicolea, J., Alfonso, F., Escaned, J., Flores, A. A., Fernandez-Ortiz, A., Banuelos, C., Hernandez-Antolin, R. A., and Macaya, C., 2002, "Implications of Late Expansion of Self-Expanding Stents on Neointimal Response: A Serial Study With Intravascular Ultrasound," Rev. Esp. Cardiol., **55**(1), pp. 16–24.
[32] Zhao, H. Q., Nikanorov, A., Virmani, R., Jones, R., Pacheco, E., and Schwartz, L. B., 2009, "Late Stent Expansion and Neointimal Proliferation of Oversized Nitinol Stents in Peripheral Arteries," Cardiovasc. Intervent. Radiol., **32**(4), pp. 720–726.
[33] Timmins, L. H., Meyer, C. A., Moreno, M. R., and Moore, J. E., 2008, "Effects of Stent Design and Atherosclerotic Plaque Composition on Arterial Wall Biomechanics," J. Endovasc. Ther., **15**(6), pp. 643–654.
[34] Colombo, A., Stankovic, G., and Moses, J. W., 2002, "Selection of Coronary Stents," J. Am. Coll. Cardiol., **40**(6), pp. 1021–1033.
[35] Liao, R., Green, N. E., Chen, S. Y., Messenger, J. C., Hansgen, A. R., Groves, B. M., and Carroll, J. D., 2004, "Three-Dimensional Analysis of In Vivo Coronary Stent–Coronary Artery Interactions," Int. J. Cardiovasc. Imaging, **20**(4), pp. 305–313.
[36] Wu, W., Wang, W. Q., Yang, D. Z., and Qi, M., 2007, "Stent Expansion in Curved Vessel and their Interactions: A Finite Element Analysis," J. Biomech., **40**(11), pp. 2580–2585.
[37] Duerig, T. W., Tolomeo, D. E., and Wholey, M., 2000, "An Overview of Superelastic Stent DESIGN," Minim Invasive Ther., **9**(3–4), pp. 235–246.
[38] Moore, J. E., and Berry, J. L., 2002, "Fluid and Solid Mechanical Implications of Vascular Stenting," Ann. Biomed. Eng., **30**(4), pp. 498–508.
[39] Gamero, L. G., Armentano, R. L., and Levenson, J., 2002, "Arterial Wall Diameter and Viscoelasticity Variability," Comput. Cardiol., **29**, pp. 513–516.